Structural Engineering and Mechanics, Vol. 8, No. 2 (1999) 165-180
DOI: http://dx.doi.org/10.12989/sem.1999.8.2.165

Cost-based design of residential steel roof systems: A case study

S.D. Rajan†, B. Mobasher‡, S-Y. Chen‡† and C. Young‡†

Department of Civil and Environmental Engineering, Arizona State University, Tempe, AZ 85287-5306, U.S.A.

Abstract. The cost effectiveness of using steel roof systems for residential buildings is becoming increasingly apparent with the decrease in manufacturing cost of steel components, reliability and efficiency in construction practices, and the economic and environmental concerns. While steel has been one of the primary materials for structural systems, it is only recently that its use for residential buildings is being explored. A comprehensive system for the design of residential steel roof truss systems is presented. In the first stage of the research the design curves obtained from the AISI-LRFD code for the manufactured cross-sections were verified experimentally. Components of the truss systems were tested in order to determine their member properties when subjected to axial force and bending moments. In addition, the experiments were simulated using finite element analysis to provide an additional source of verification. The second stage of the research involved the development of an integrated design approach that would automatically design a lowest cost roof truss given minimal input. A modified genetic algorithm was used to handle sizing, shape and topology variables in the design problem. The developed methodology was implemented in a software system for the purpose of designing the lowest cost truss that would meet the AISI code provisions and construction requirements given the input parameters. The third stage of the research involved full-scale testing of a typical residential steel roof designed using the developed software system. The full scale testing established the factor of safety while validating the analysis and design procedures. Evaluation of the test results indicates that designs using the present approach provide a structure with enough reserve strength to perform as predicted and are very economical.

Key words: steel roof truss; full-scale testing; design curves; finite element analysis; optimal design.

1. Introduction

Use of steel roof systems for residential buildings is becoming increasingly cost effective. This is attributed to the decrease in manufacturing cost of steel components, reliability and efficiency of steel construction, and the fluctuations and uncertainties in the wood market. While steel has been a primary material for structural systems, it is only recently that its use for residential buildings is being explored. The focus of the current research is on the three aspects of development, design, and verification of guidelines for steel components. The first aspect deals with the evaluation of thin gage steel sections as the primary load bearing members. Experimental

† Professor
‡ Associate Professor
‡† Graduate Assistant

techniques are used to evaluate the load-carrying capacity of the individual cross-sections under compression, tension, and bending loads. Guidelines for connections are also established leading to the generation of design criteria for both members and connections. The second focus area is directed toward development of an automated optimal design methodology that would yield the lowest cost truss while satisfying the design code and other requirements. The last focus area is on the validation of the developed analysis and design procedures using full-scale truss testing.

Traditionally, allowable stress design (ASD) method has been used in the design of cold-formed sections. The load and resistance factor design (LRFD) criteria has also been developed for both hot-rolled (AISC: Load and Resistance Factor Design, 1986) and cold rolled steel sections (Hsiao, Yu and Galambos, 1990). Additional experimental work has been carried out by Weng and Pekoz (1990) to characterize the compression response of cold-formed steel columns. In the present work, guidelines for the AISI-LRFD design of cold-formed members in terms of tension, compression, bending, lateral buckling, shear, and web crippling strengths in addition to the interaction of axial, bending, and web crippling are used to develop the design curves. Although the proposed approach is applicable to a variety of structural members, systems, and geometrical shapes, the discussion is limited to roof truss systems as a general structure. Mechanical tests were conducted at the component level to evaluate the performance of the individual members under the different loading conditions of compression, flexure, and tension. The experimentally obtained failure loads were compared to the values from the AISI code as well as from finite element analysis. The motivation here is to ensure that the design curves based on the AISI-LRFD code requirements are applicable to the cross-sections being used and do not lead to unsafe design practices. It should be noted that the AISI-LRFD based design curves are then used in an automated design process to check the adequacy of each design while finding the truss with the lowest cost. To validate the design process and methodology, a full-scale test was conducted for the truss design with the lowest cost.

The major components used as truss members consist of closed and open sections. In this study, standard sections manufactured by Allied American Inc., Phoenix, Arizona were used. Fig. 1 shows the typical (open) chord cross-section and the (closed) hollow square cross-section. A single shape, open C-section with stiffened edges at two different web depths and three different

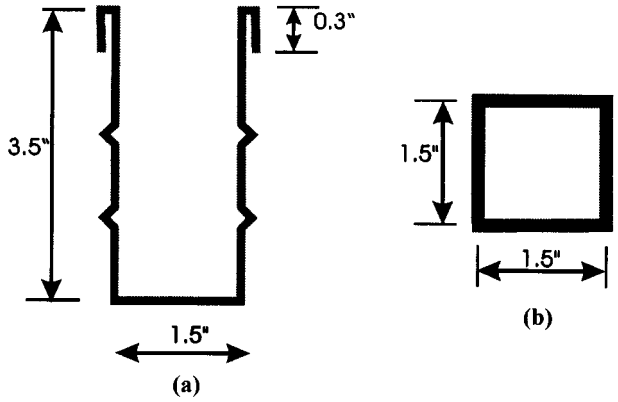

Fig. 1 (a) Typical chord section (designation: 3.5 CHORD 16GA, also available as 2.5" deep section and gages 18 and 20), (b) square section for web and heel section (designation: 1.5 SQWEB 16GA, also available in 18 and 20 gages)

gages were tested and used. Web depths were 2.5" and 3.5", and three plate thicknesses or gages were 16 GA., 18 GA. and 20 GA. The open C-sections were used for the top and bottom chords. The closed sections were standard rectangular square tube (of sides 1.5") of different gages. These sections were used for the design of the heels, King Post and web members.

The paper is organized into three sections. The first part discusses the verification of the design curves. This is followed by a discussion of the optimal design methodology used in designing the lowest cost truss. Results from a specific example are discussed. This specific design is then used in the full-scale test that is discussed in the final part of the paper.

2. Construction and validation of the AISI-LRFD design curves

Design curves provide the range of internal forces that can be allowed in any member as a function of its geometrical constants and length. They can then be used as a part of the automated software in the design of the truss members. In this study, the design curves for the open sections were developed in three independent ways. The motivation is to ensure that the AISI code based values are applicable to the chosen cross-sections with adequate factor of safety. Initially, mechanical testing was carried out on replicates of individual members of several lengths. Next, finite element simulations of the axial and bending response were conducted. Finally, the AISI-LRFD code was used to compute the design curves, i.e. allowable force versus unbraced length charts (AISI 1986).

2.1. Mechanical tests

The tests conducted included flexural, compression and tension tests. Using two different web depths of 2.5 and 3.5 inches at three different gages of 16, 18, and 20 resulted in six different specimen types. Axial strain in certain specimens was measured using resistance type strain gages. One strain gage was placed at the mid-length of the specimen on the outside of the flange. The load, elongation, and strains were continuously recorded using a data acquisition system with 12 bits resolution. Digital data analysis was used to reduce the data and analyze the test results.

2.1.1. Axial compression tests

In the compression test, for each specimen type, four replicate samples for each of the four lengths of 12, 24, 36, and 48 inches were tested. Tests were performed on a closed loop servohydraulic test machine with a capacity of 220 kN (55 kips). The specimen ends were attached to the load frame by means of a rigid connection. The test machine was controlled using the TestStarII software package developed by MTS Corp (Minn, MN). A constant displacement rate was applied to the end plate while the load was measured using a load cell. The displacement of the actuator was used as the control parameter and prescribed to increase at a specified rate of 0.1" per minute. For each test, the compressive load versus end displacement were measured. Fig. 2 shows the load-displacement response of four 2.5" 18 GA chord section specimens (12" through 48") as a function of length. Similar response was obtained from other specimen types. For short specimen lengths, failure is governed by the crushing of the specimen at the loaded ends or local buckling. For the longer specimens, the buckling is controlled by primarily an Euler type buckling. Regardless of the mode of failure, tests were continued well beyond the ultimate load magnitude to measure the post buckling capacity. Ultimate load carrying capacity of a component is defined

as the maximum load that could be sustained by the component under uniaxial or flexural load.

Due to the presence of residual stresses, there is a gradual transition from one mode to the other as the length of the specimen increases. Due to the displacement-controlled mode of loading, it was possible to extend the testing well beyond the ultimate load capacity. In this manner, the post buckling load carrying capacity was measured as well. In many instances, this capacity represents a significant fraction of the overall load carrying capacity of the section. Such load carrying capacities are accounted for neither in the theoretical calculations nor the AISI-LRFD code. This adds to the conservatism in the design methodology.

Fig. 2 shows initially a linear response as the applied displacement uniformly stresses the sample. The stiffness of the samples is inversely proportional to their length. As the load increases, the response of specimen deviates from linearity and local buckling initiates in the short samples. The 12" and 24" sections behave similarly up until the 8000 pounds level, where local buckling initiates. Beyond this point, the local buckling in the 24" sample dominates, and the load carrying capacity diminished altogether. The 12" sample however continues to carry further load and increases in load carrying capacity up to 12000 pounds. This stress level corresponds roughly to 20 ksi and signifies the fact that residual stresses are present in the sample due to the forming process. Since the test was conducted under constant displacement rate, the failure of the specimen was gradual. As large deformations accumulate due to global or localized buckling, the servo-loop control system reduced the load so that the rate of displacement is maintained equal to the prescribed level. The test was terminated at a predetermined displacement. This displacement level was chosen as 0.5" for the 18 and 20 GA specimens, and 0.6" for the 16 GA specimens.

Fig. 3(a) shows the individual data points from specimens tested as well as the mean value for each tested length. While the 3.5" deep chord sections were also tested, the ultimate loads obtained for each sample of the three gages studied are shown in the plot for the 2.5" chord section only. The error bars indicate the standard deviation of the mean of the samples tested in each category. A curve that fits the mean values of these test results indicates the trend of the

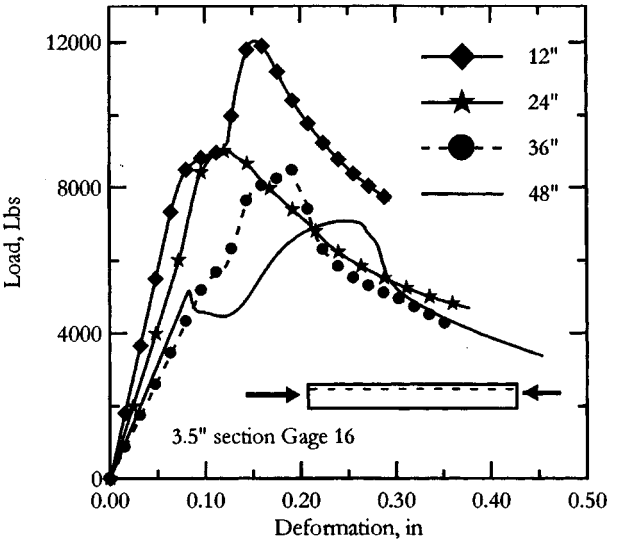

Fig. 2 Load-displacement curve for 2.5 CHORD 18GA 12" to 48" specimens during axial compression test

reduction in ultimate load as a function of unsupported length. It should be noted that the ultimate load carrying capacity is also a function of the effective length of the specimen. Since the specimens were rigidly attached to the test frame at the ends, the effective length is given as $KL = 0.5L$ where L is the specimen or unsupported length.

Fig. 3(b) shows another important facet of the test results for the two extreme specimen lengths - 12" and 48". The nominal stress at the ultimate load is plotted against the w/t ratios of the different specimens. Curve-fitting using the data points yields the solid lines. The longer length (48") shows little variation (with respect to the gage, section depth and length) of the nominal stress in the cross-section at the ultimate load value. This is because of the Euler buckling phenomenon (that governs failure) that is more a function of the length than the w/t ratio. The shorter length (12") is relatively insensitive to the specimen parameters for the thicker section (16 GA). However, the nominal stress decreases (or, the ultimate load carrying capacity decreases) with increasing w/t values due to the local buckling phenomenon.

2.1.2. Flexural tests

A four-point bend test fixture was developed for the flexural test to eliminate extraneous deformations such as support settlements and specimen rotations. The objective of this test was to compute the maximum positive and negative bending moment (torsional buckling prevented) that the sections can withstand assuming that member is sufficiently short and under braced conditions. A span length of 24" was chosen to achieve this purpose. Positive moment is defined as causing compression in the flange whereas negative moment caused tension in the flange.

The specimens were simply supported on the loading fixture. Two line loads spaced at 4.75" apart were used to apply the flexural forces. In order to prevent local crushing of the specimen due to stress concentration, steel plates 1/4" in thickness were used under the loading points.

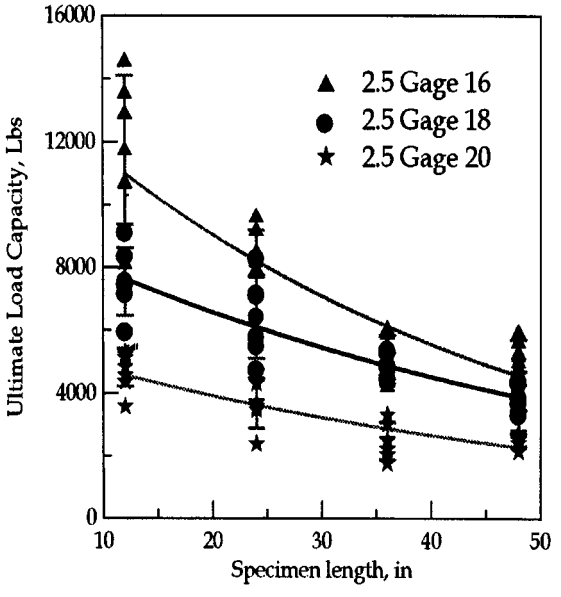

Fig. 3(a) Experimentally obtained mean ultimate load carrying capacity for different 2.5" chord specimens

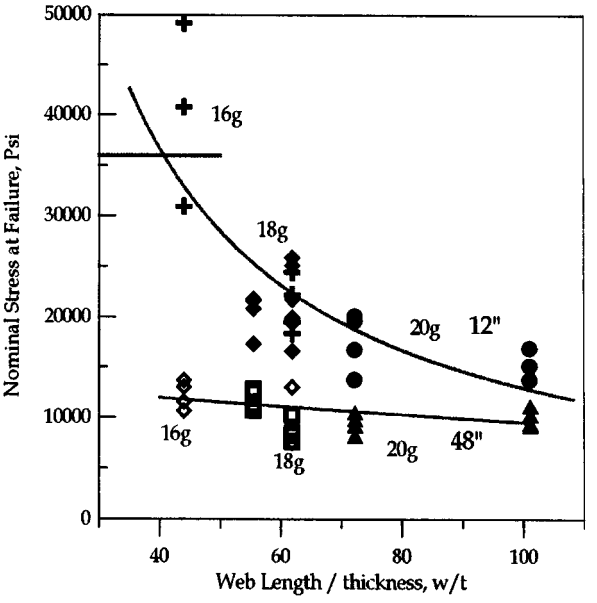

Fig. 3(b) Experimentally obtained nominal stress at failure versus w/t for different specimens

Specimen deflections were measured using a Linear Variable Differential Transformer (LVDT). Two replicate tests per section were conducted for each positive and negative bending moment tests. The test was terminated in the post peak region of the response when the vertical displacement exceeded 0.8" for negative moment and 0.4" for positive moments. The maximum bending moment, M_{max} was calculated as:

$$M_{max} = \frac{Ps}{2} \tag{1}$$

where s is the distance from the support to the point of application of the load and P is the maximum applied load.

2.2. Finite element simulations

As an alternate approach to verify the test results and the AISI guidelines, the finite element method was used to compute the elastic buckling strength of the members. An eigenvalue problem was formulated using a procedure of linearized buckling analysis as follows: The current nodal forces are P^N where N is the number of degrees of freedom in the structure. The corresponding elastic tangent stiffness matrix is K_P. Addition of nodal loads Q^N causes the loading state to reach P^N+Q^N while the elastic stiffness changes to K_Q such that $K_Q=K_P+\lambda\Delta K_{PQ}$. The term ΔK_{PQ} is the change in stiffness going from one stage to the other and is assumed proportional to the change in the load Q^N. This assumption is valid for stiff structures that undergo only small rotations prior to buckling. The tangent stiffness matrix at a load state $P^N+\lambda Q^N$ is predicted as $K^P+\lambda\Delta K_{PQ}$. Thus the load rate-displacement relationship is (HKS 1995).

$$(K_P^{NM} + \lambda\Delta_{PQ}^{NM})\, du^M = dF^N \tag{2}$$

The non-trivial solutions to this system as an eigenvalue problem is when $dF^N=0$, or

$$(K_P^{NM} + \lambda\Delta K_{PQ}^{NM})\, du^M = 0 \tag{3}$$

The buckling load is estimated as

$$P^N + \lambda_i Q^N \tag{4}$$

with du_i^N as the buckling mode.

To simulate the compressive tests, the specimens of different lengths were modeled using 4-noded thin shell elements with 6 degrees of freedom per node. No initial loads were applied (P^N= 0) and the axial compressive load was used as the buckling variable. The boundary conditions at the end conditions were designated as fixed to match the experimental setup. A parametric study was carried out to find the optimal mesh layout. Solution of the finite element analysis giving the lowest eigenvalue was used to calculate the compressive buckling axial force (Eq. (4)). A similar finite element simulation was conducted for the four-point bending test. However, in this case the load was taken as the two-equal and opposite line loads applied at a distance from the ends.

2.3. AISI-LRFD calculations

Finally, the AISI-LRFD design code (AISI 1986) was used to compute the corresponding values of the different cross-sections. The details of the code provisions and the relevant

calculations are not shown here since they are not the primary focus of the current study. They are however available in a research report (Mobasher and Situ 1996).

2.4. Comparison of the obtained values

The following sections provide a comparison of the different values obtained using the laboratory test procedure, finite element simulations and the AISI-LRFD design code.

2.4.1. Axial compression

The values obtained from the laboratory (denoted as experimental mean), AISI-LRFD design code and finite element analysis (denoted FEA) for the axial compression tests are compared in Table 1.

The visual comparison is presented in Fig. 4 for the 3.5" 16GA specimens. The ultimate load capacity, as expected, decreases with increasing length. While three of the four curves are for the case where the ends of the specimen are assumed to be fixed, an additional curve shows the effect of the using pins (or moment release hinges) at the ends (K=1.0). The other specimen types exhibit similar behavior.

2.4.2. Bending

The values obtained from the laboratory, AISI-LRFD design code and finite element analysis for the four-point bending tests are compared in Table 2.

2.4.3. Discussion of the results

The following points are noted when comparing the results obtained from the three different approaches:

(1) The experimental values are higher than either the AISI or the FEM values for all but two specimen types (they are however, within 2% and 10%). The experimental values reflect

Table 1 Comparison of results for the axial compression test

		Ultimate Load (lb)					
		3.5 CHORD			2.5 CHORD		
Length	Source	20 GA	18 GA	16 GA	20 GA	18 GA	16 GA
12"	AISI-LRFD	3176	4376	7035	3224	4447	7176
	FEA	3290	5359	8432	3623	6256	9726
	Exp. Mean	4900	9643	11488	4576	6979	11296
24"	AISI-LRFD	2729	3729	5788	3071	4200	6706
	FEA	2353	3932	6371	2896	4814	8061
	Exp. Mean	4852	8039	9593	4052	7065	8696
36"	AISI-LRFD	1882	2624	3776	2788	3800	5918
	FEA	2007	3554	5874	2712	4528	6635
	Exp. Mean	4203	6953	7785	2727	5090	5342
48"	AISI-LRFD	1259	1765	2576	2353	3224	4835
	FEA	1908	3396	5415	2313	3252	4505
	Exp. Mean	3324	3755	8143	2477	4049	5279

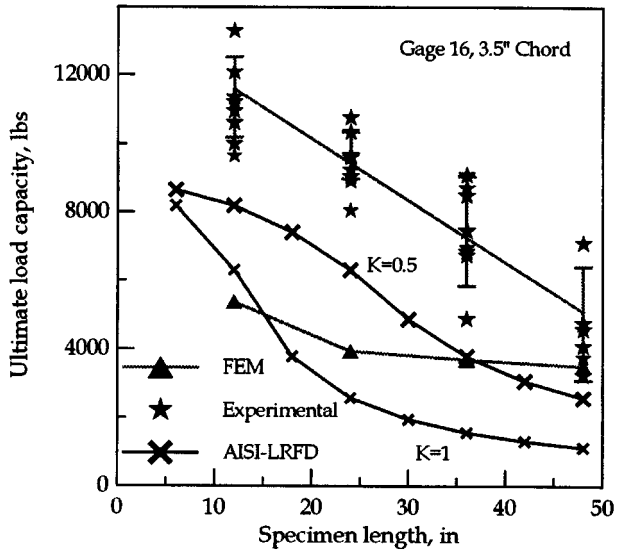

Fig. 4 Comparison of ultimate load capacity versus specimen length values for 3.5 16GA chord section

the peak value from the load-displacement curve. The post-peak strength is quite significant providing additional reserve stiffness and strength in the case of a design of a structure with redundancies. For systems with sufficient redundancy, the reserve strength may improve the factor of safety against overall failure. This behavior is not directly considered in a linear elastic based design.

(2) The deflection and deformation at peak load obtained from the experimental approach is significantly higher than the values obtained from the equivalent elastic approach. This is due to pre-peak nonlinearities observed in the experimental data as shown in Fig. 2.

(3) The FEA values are larger than the AISI values for 19 out of the 24 cases for the Axial Compression Tests and for all the cases for the Four-Point Bending Tests. In cases where

Table 2 Comparison of results for the four-point bending test

	Positive Moment Capacity (lb-ft)					
	3.5 CHORD			2.5 CHORD		
Source	20 GA	18 GA	16 GA	20 GA	18 GA	16 GA
AISI-LRFD	81	122	209	80	120	204
FEA	159	276	487	205	320	512
Exp. Mean	430	739	1027	382	668	860
	Negative Moment Capacity (lb-ft)					
	3.5 CHORD			2.5 CHORD		
Source	20 GA	18 GA	16 GA	20 GA	18 GA	16 GA
AISI-LRFD	237	320	497	250	338	529
FEA	304	465	764	308	489	809
Exp. Mean	602	1047	1576	483	822	1212

the FEA values are smaller than the AISI values, only one sample was more than 6% lower than the corresponding AISI value.

(4) The finite element based linearized buckling analysis is closer to the experimental values for cases with longer column lengths where the column follows an Euler buckling behavior. This may be attributed to the mesh refinement issue in the capturing of the local buckling modes.

(5) In conclusion, the use of the AISI-LRFD design code values provides conservative design values for the section sizes and lengths used in the present study. These AISI-LRFD Code guidelines were used in the subsequent sections for the design of the truss components.

3. Optimal design of truss

Several methodologies exist for optimal design of discrete structures such as trusses and frames. The methodology used in the present design of the roof truss is based on simultaneous sizing, shape, and topology design using genetic algorithm (GA) as the optimizer as discussed in Wright *et al.* (1995) and Chen and Rajan (1998).

The LRFD strength requirements for each member type were calculated based on the AISI specifications as a function of the unbraced length of the section. This ultimate strength versus section length curve was subjected to piecewise linear approximations describing the strength envelope curve. After a single finite element analysis was conducted, the forces in the member and its length were compared to the strength envelope data and the distance form the envelope curve were calculated. If the point corresponding to the member forces and length fell inside the curve, no penalty was assessed. If it fell outside the curve, the penalty term was calculated as

$$f_{penalty} = c\left(\frac{v}{v_a} - 1\right) \tag{5}$$

The term in the parenthesis represents the normalized distance to the curve and c is the penalty parameter. The finite element analysis was conducted next in an effort to achieve a design such that each element is within the safe strength envelop and the penalty factor is reduced. This would ensure a safe design approach. To achieve an optimum design, the number of elements, and the cost of members must be minimized as well. The roof truss design problem is formulated as follows. The objective function is defined as the cost of the truss given as

$$f(x) = \sum_{j=1}^{ne} c_j L_j + \sum_{k=1}^{nj} d_k + \sum_{l=1}^{nc} e \tag{6}$$

where ne is the number of elements, nj is the number of joints, nc is the number of cuts made to obtain the truss members, L_j is the length of the element j, c_j, is the cost per unit length, d_k is the cost of the connection (a function of the number of screws needed to construct the connection), and e is the cost of making a cut in a cold-rolled specimen so as to obtain a specified length member. The first term captures the material cost whereas the second and the third terms account for the labor cost.

The general steps followed in the design procedure are as follows:

(1) The design process is initiated by specifying the geometrical and loading parameters. These include the span, height of the King Post (or, the pitch of the roof), the dead and live loads acting on the top and bottom chords, heel heights and support conditions, the overhangs,

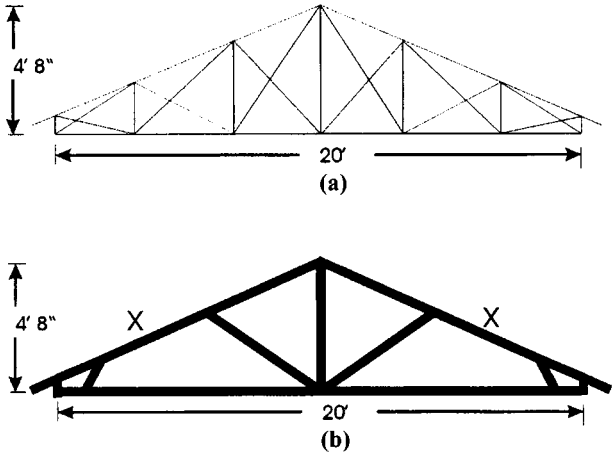

Fig. 5 (a) Initial guess, (b) the lowest cost truss obtained from the optimal design process

from side sway buckling or tipping over. In order to achieve these tasks, a three-truss system was assembled based on the design obtained in the preceding section. The trusses were placed 2' apart. They were joined continuously at the top chord using 0.5" thick plywood sheathing. Hat channels were used at 5' spacing to connect the bottom chords of the trusses as well. The single sheet of 0.5" thick plywood acted as the roof element. Dead load was applied in incremental stages over the length of the top chord members by means of 50 lb sand bags. The bags were manually weighed and placed in several layers. In between each loading sequence, the response of the truss in terms of the applied load, the measured loads, the deflections, and strains in the members were recorded.

4.1. Test details and results

The instrumentation details as shown in Figs. 6(a)-(b) represent the front and side view of the test assembly. Due to the nature of loading shown in Fig. 6, only the middle truss is tested to failure by placing an equivalent dead load on the tributary roof area. The locations of the six load cells and three deflection dial gauges are shown In Fig. 6(a). The center truss spans the load cells labeled W2-E2 and the dial gauges labeled W, C and E.

The truss loading was continued until a satisfactory level of factor of safety with respect to the design loads was achieved. This was achieved while there were no visual signs of failure in a member or at a joint. The testing was terminated when it was determined that the allowable safety factors were reached, and that additional forces on the truss could affect its load carrying capacity by means of a sudden uncontrollable failure, causing safety concerns.

Table 3 shows the loads placed at different stages of the test and gives an idea as to how the loads are distributed between the three trusses. The second column represents the weight of the sand bags as measured individually before being placed on the truss. The third column shows the load on all the trusses as measured by the load cells placed at the bottom of the heels of the trusses. The deflection of the truss was recorded using dial gages with a resolution of 0.001" and a range of 1" throughout the loading history. The deflection was measured at three nodal points on the bottom chord. Fig. 7 represents the total load applied vs. the deflection response of the truss. As shown in the figure, the deflection of the bottom chord member is quite uniform

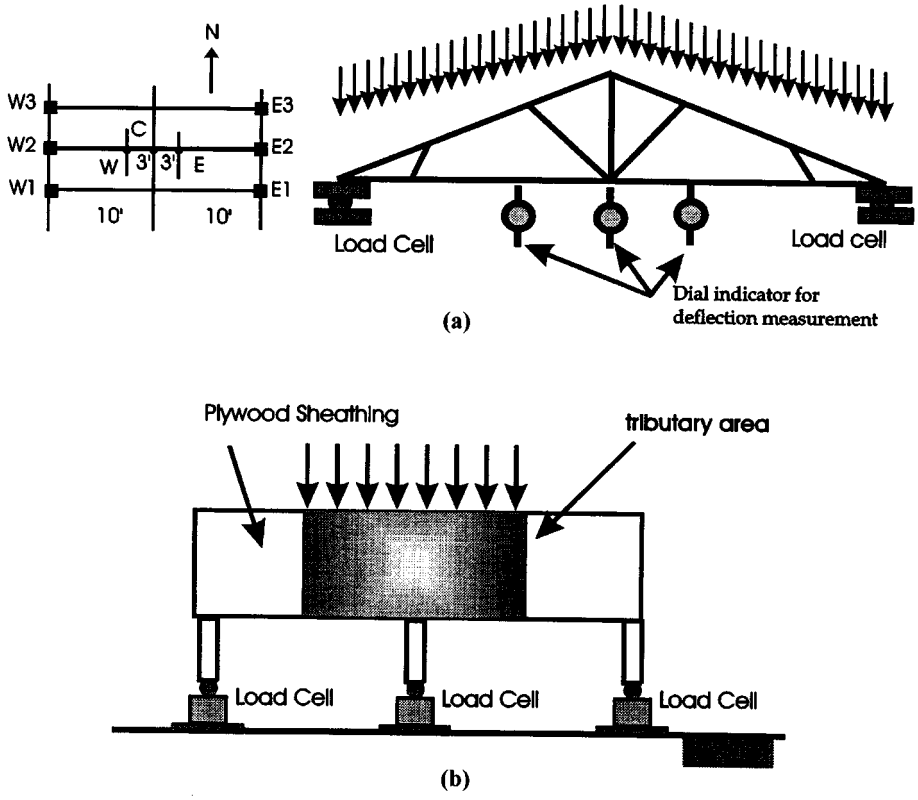

Fig. 6 (a) Schematics of the instrumentation of the truss, load cells, and dial gauges, (b) Side view of the three truss assembly system

throughout the length of the member for a major portion of the load applied. An initial linear response is seen until about 1600 lbs. The slopes of the curves change at this point and the second nearly linear response is observed until about 2500 lbs. Beyond that point, the response is nonlinear.

The axial strains of several truss members were measured using resistance type strain gages that were placed at the center of the member on the side indicated in Table 4. A total of 7 members were monitored throughout the test duration. The strain gage data were collected using a data acquisition system. Fig. 8 represents the axial strain in six members. It should be noted that the strain in these members remains relatively low as the truss is loaded.

The measured strains and deflections are compared to the FEA strains and deflections in Table 4(a). This is done in order to measure the effectiveness of the structural model in predicting the response of the truss. A linear FE analysis was carried out to design the truss. An obvious question is whether a linear analysis is adequate. The results in Table 4 indicate that while the strains and deflections are both quite small, there are noticeable differences in the experimental versus FE values. Alternate FE models could be investigated to better predict the structural response. To enable better predictions, an elastic-perfectly plastic FE model was created and analyzed using ANSYS (ANSYS 1997). The purpose of the elasto-plastic model was to cap the load carrying capacity of a member when the normal stress anywhere in a member exceeded the nominal stress value shown in Fig. 3(b). This is the stress level at which buckling takes place, a

Table 3 Load cell and deflection readings

Loading Stage	Applied Load (lbs)	Load Cell Readings (lbs)						Deflection Readings (in)		
		W1	W2	W3	E1	E2	E3	W	C	E
Initial	0	0	0	0	0	0	0	-	-	-
Stage 0	387	47	95	48	48	95	50	0.011	0.013	0.012
Stage 1	392	96	196	98	98	184		0.026	0.030	0.028
Stage 2	389	135	319	126	135	293		0.046	0.042	0.046
Stage 3	397	180	431	169	178	398		0.064	0.059	0.062
Stage 4	403	227	541	212	224	523		0.087	0.085	0.087
Stage 5	393	273	654	256	264	605		0.117	0.112	0.119
Stage 6	382	321	749	304	308	709		0.153	0.145	0.155
Stage 7	380	362	856	349	350	806		0.211	0.204	0.217
Stage 8	393	454	983	396	398	881		0.276	0.269	0.287
Stage 9	403	439	1092	444	449	995	426	0.335	0.319	0.339
Stage 10	391	489	1192	487	497	1094		0.397	0.380	0.402
Stage 11	258	511	1268	516	524	1174		0.423	0.406	0.426
Stage 12	375	563	1356	570	576	1244		0.492	0.481	0.504
Stage 13	366	612	1444	609	631	1341		0.558	0.550	0.573
Stage 14	296	646	1533	655	672	1375		0.630	0.625	0.649
Stage 15	336	673	1629	700	707	1466		0.664	0.656	0.687
Stage 16	296	699	1719	745	742	1563	725	0.704	0.697	0.737
Total Load (lbs)	**6237**			**6193**						

phenomenon that cannot be captured in the linear model. This analysis was carried out. Furthermore, addition of geometrically nonlinear effects to this ANSYS model did not change the final response. This is to be expected since the overall deflections in the truss are very small. The final results indicated that the number of elements exhibiting the "elasto-plastic behavior" is relatively small and is confined to the four elements in the top and bottom chords around the left and right heels. The stress in the overhangs is small and the heels are relatively strong.

4.2. Discussion of the test results

The following observations are pertinent regarding the distribution of the load and the test results. At the time of termination of the test, there were no visual member or joint failures observed in the center truss. The combined load cell readings for the center truss was 3282 lbs. The design load was based on a total load of 1840 lbs. Based on the ratio of applied load to design load, the factor of safety for the truss used in the full-scale test is at least 1.8.

(1) A comparison of the center truss load cell readings (W2 versus E2), shows that the load distribution is fairly even on both sides of the truss. The maximum level of deviation of load distribution was 10% at Stage 14.

(2) A comparison of the load cell readings for the outer trusses (W1, W3, E1 and E3) shows that the load distribution is fairly even to the outer trusses with a maximum difference of about 6% at Stage 16. Hence, load calculations based on the tributary areas are deemed to be adequate.

(3) The difference between the load applied on the truss (the sandbags were weighed individually

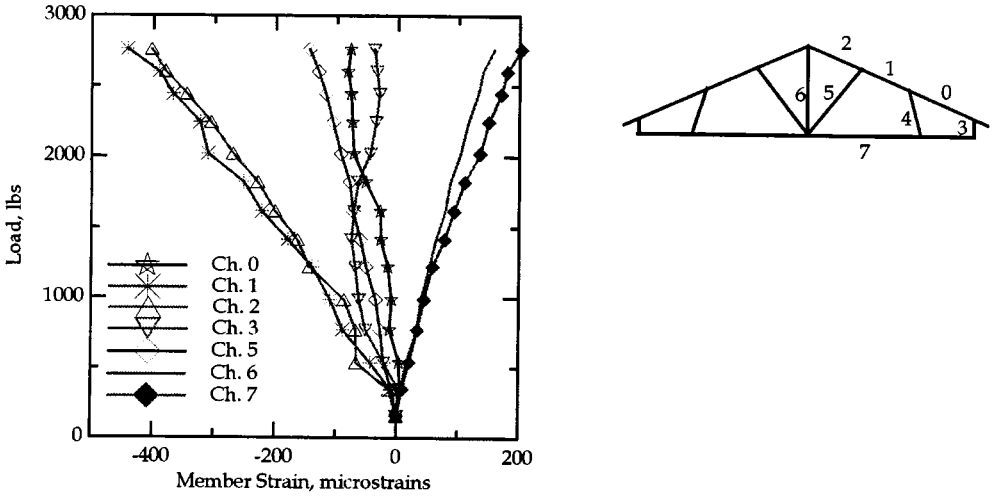

Fig. 7 Member strain versus total load for select members in the center truss

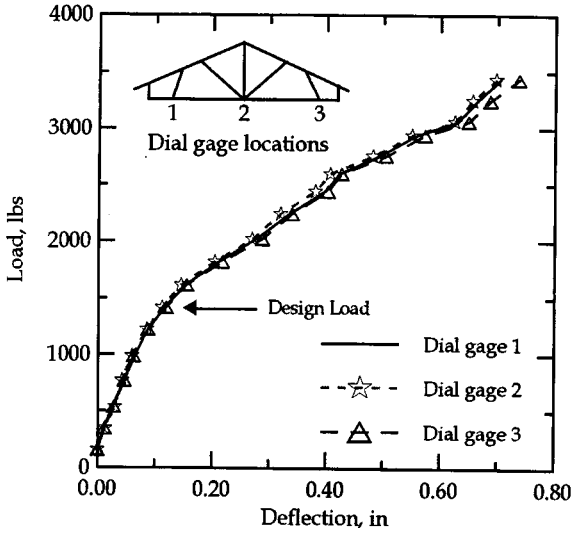

Fig. 8 Bottom chord deflections of the center truss versus total load applied on the center truss

Table 4(a) Comparison of experimental (1864 lbs; Stage 8) and FEA (1840 lbs) strain values for the center truss (Micro-strains)

Channel	Experimental	Linear FEA	Difference[4] (%)	Nonlinear FEA	Difference[4] (%)	Gage Position
0	-52	-45	-14	-42	-15	TOP
1	-252	-160	-37	-245	-3	TOP
2	-229	-160	-37	-194	-15	TOP
3	-65	-55	-15	-65	0	LEFT
4	bad	-81	-	-114	-	LEFT
5	-78	-33	-58	-27	-65	RIGHT
6	87	68	-22	52	-40	RIGHT
7	110	208	90	152	38	BOTTOM

[4]Using experimental value as the basis

Table 4(b) Comparison of experimental (1864 lbs; Stage 8) and FEA (1840 lbs) vertical displacement values for the center truss (in)

Location	Experimental	Linear FEA	Nonlinear FEA
Bottom of King Post	0.269	0.08614	0.228

before being placed the roof) and the load cell readings was indeed very small. At Stage 16, the difference was less than 1% (6237 lbs measured versus 6193 lbs combined reading of the six load cells). This indicates that the system was well instrumented, and all the various load distribution mechanisms were accounted for.

The differences in the load cell readings can be attributed to several reasons. The roller versus the pin support conditions at the base of the heels cannot be realized in the laboratory. The seating of the truss takes place as the truss is loaded. During the major portion of the loading history, it was observed that the two ends of the truss equally participate in carrying the vertical loads. Towards the end of the test where non-linear effects become dominant, the two load cell responses show the variations with more force being carried by the hinge support.

To summarize the following conclusions and observations can be made.

(1) The FEA model is two-dimensional whereas the full-scale test incorporates three-dimensional effects such bracing and load transfer through the braces. The two-dimensional model does not incorporate the stiffening and load distributing effects of the plywood sheeting nor does it detect and account for the effects of local buckling. While the nonlinear FEA model yielded results closer to experimentally obtained values, analysis and design based on a linear FEA model is acceptable since the magnitude of the maximum displacement and the extent of inelastic behavior are both small. Furthermore, as mentioned above the tributary load transfer mechanism is validated as per the full-scale test results. A full three-dimensional analysis (including the modeling of the plywood sheeting and the lateral bracing on the bottom chord) is likely to be an overkill.

(2) The planar FEA model assumes that all the joints are rigid connections. In reality, the joints are somewhere between a rigid connection and a pin connection.

(3) During the testing, the bottom chord members were laterally braced. In the FEA model, no bracing is assumed. This may explain why the FEA models overpredict the axial strain (Channel 7). It should be noted that in comparing the experimental to FEA results, the order of the error in the measured values is not known even though it has been used as the basis of comparison.

5. Concluding remarks

A comprehensive system has been developed to design residential steel roof truss systems. The AISI-LRFD design code is used in the design process. The major AISI design curves that are applicable have been checked using experiment values as well as using finite element simulations. A GA-based design methodology has been developed that uses minimal input to automatically size, shape and configure the truss. The analysis and design processes are tested using a full-scale test of a 20' span, flat-bottom truss. The summary of the research accomplishments is as follows:

(1) Development an automated design procedure to design the lowest cost truss. The design procedure includes (a) the planar frame structural analysis carried out to compute the response

of the individual members subjected to the design loads; (b) use of the response values in an AISI-based design checks to ensure the adequacy of the individual members; and (c) the procedure to redesign in order to minimize the cost of the truss.

(2) The validity of the structural analysis is established by comparing the linear and elasto-plastic FEA models' strain and deflection values against the values obtained from the full-scale test.

(3) The validity of the design checks and design curves are established by computing the factor of safety, and comparing the actual mode of failure to the predicted mode of failure. Since the truss did not fail even at a load level of 1.8 times the design load, the design curves used for the design are deemed to be adequate.

(4) The procedure to redesign the truss in order to obtain the lowest cost truss is validated by comparing the cost of the truss to industry norms. The cost of the designed truss is $51 translating to about $2.50 per linear foot. This is about the best estimated cost as per industry norm. These final designs are obtained with minimal user input and in a reasonable amount of computer time.

Acknowledgements

The research sponsorship of Allied American Inc., Phoenix, AZ is greatly appreciated. Special thanks to Allied American personnel - Robert Dixson, Matt Watson, Mike Meek, Dan Dry and Paul Shumway, for their contributions during the different stages of the research. Special mention should also be made of graduate students Joanne Situ, Dmitri Wright and Garrett Haupt for their invaluable assistance in generating the design curves and conducting the full-scale testing.

References

American Institute of Steel Construction (1986), *Load and Resistance Factor Design Specification for Structural Steel Building.*

American Iron and Steel Institute (1986), *AISI LRFD Cold-Formed Steel Design Manual, Part 1: Specification for Cold-Formed Steel Structural Members.*

ANSYS, Inc. (1997), ANSYS Theoretical Manual.

Chen, S-Y. and Rajan, S.D. (1998), "Improving the efficiency of genetic algorithms for frame designs", *Engineering Optimization,* **30**, 281-307.

HKS, Inc. (1995), ABAQUS Theoretical Manual.

Hsiao, L-E, Yu, W-W and Galambos, V. (1990), "AISI LRFD method for cold-formed steel structural members", *ASCE J of Structural Engineering,* **116**, 500-517.

Mobasher, B. and Situ, J. (1996), ICBO Test Report of the American Studco, Inc., Residential Roof Truss Chord Components, Report No. CEE-AS-95-1, Dept. of Civil Engineering, Arizona State University.

Rajan, S.D. (1995), "Sizing, shape and topology design optimization of trusses using a genetic algorithm", *ASCE J, Structural Engineering,* **121-10**, 1480-1487.

Salmon, C. and Johnson, J. (1990), *Steel Structures: Design and Behavior*, Harper Collins Publishers, New York.

Weng, C.C. and Pekoz, T. (1990), "Compression tests of cold-formed steel columns", *ASCE J, of Structural Engineering,* **116**, 1230-1246.

Wright, D., Situ, J., Mobasher, B. and Rajan, S.D. (1995), "Development and implementation of an automated design system for steel roof trusses", *Proc. Research Transformed Into Practice: Implementation of NSF Research*, Eds. Colville and Amde, ASCE Press, Washington, D.C., 245-256.